Histone H2A.Z cooperates with RNAi and heterochromatin factors to suppress antisense RNAs

Martin Zofall[1,*], **Tamás Fischer**[1,*], **Ke Zhang**[1], **Ming Zhou**[2], **Bowen Cui**[1], **Timothy D. Veenstra**[2], and **Shiv I. S. Grewal**[1]

[1]Laboratory of Biochemistry and Molecular Biology National Cancer Institute National Institutes of Health Bethesda, MD 20892

[2]Laboratory of Proteomics and Analytical Technologies, Advanced Technology Program, SAIC-Frederick, Inc., NCI-Frederick, Frederick, MD 21702

Abstract

Eukaryotic transcriptomes are characterized by widespread transcription of non-coding and antisense RNAs[1–3], which is linked to key chromosomal processes, such as chromatin remodeling, gene regulation, and heterochromatin assembly[4–7]. However, these transcripts can be deleterious, and their accumulation is suppressed by several mechanisms including degradation by the nuclear exosome[8,9]. The mechanisms by which cells differentiate coding RNAs from transcripts targeted for degradation are not clear. Here we show that the variant histone H2A.Z, which is loaded preferentially at the 5' ends of genes by the Swr1 complex containing a JmjC domain protein, mediates suppression of antisense transcripts in the fission yeast *Schizosaccharomyces pombe* genome. H2A.Z is partially redundant in this regard with the Clr4/ Suv39h-containing heterochromatin silencing complex that is also distributed at euchromatic loci, and with RNAi component Argonaute (Ago1). Loss of Clr4 or Ago1 alone has little effect on antisense transcript levels, but cells lacking either of these factors and H2A.Z show markedly increased levels of antisense RNAs that are normally degraded by the exosome. These analyses suggest that in addition to performing other functions, H2A.Z is a component of a genome indexing mechanism that cooperates with heterochromatin and RNAi factors to suppress read-through antisense transcripts.

Histones are a major structural component of chromatin, critical for packaging and regulation of eukaryotic genomes. Specialized chromatin can be differentiated by local incorporation of variant histones into a subset of nucleosomes[10]. A conserved variant histone, H2A.Z has been linked to diverse chromosomal processes[10], but its specific

regulatory function(s) are unclear. Although H2A.Z is dispensable for viability in *S. cerevisiae*, it is essential in *Drosophila* and mice, where it is linked to both transcriptional activation and repression[10,11]. Evidence suggests that metazoan H2A.Z localizes to heterochromatic loci and its depletion causes defective chromosome segregation[12].

In this study, we used *S. pombe* to explore H2A.Z functions. *S. pombe* genome contains large blocks of heterochromatin, whose assembly requires histone H3 lysine 9 (H3K9)-specific methyltransferase Clr4/Suv39h, Swi6/HP1 family proteins, and the RNAi machinery[7]. Deletion of *pht1*, the gene encoding H2A.Z causes segregation defects[13]. However, it is not known whether this phenotype is linked to defective heterochromatin.

H2A.Z deposition is catalyzed by the Swr1 complex in *S. cerevisiae*[10]. To establish if a similar complex deposits H2A.Z in *S. pombe*, we purified factors associated with H2A.Z and Swr1 homolog. These analyses identified an analogous complex in *S. pombe*, which also contained a JmjC domain protein, Msc1 (Supplementary Fig.1)[14]. Msc1, while dispensable for complex assembly (Supplementary Fig. 1), affected chromatin association of Swr1 (Fig. 1a). Both Swr1 and Msc1 were required for H2A.Z deposition at various sites, though *swr1* was more defective (Fig.1b; Supplementary Fig. 2a–d).

ChIP-chip analysis showed a non-random distribution of H2A.Z across the genome (Supplementary Fig. 2c). H2A.Z is relatively depleted throughout heterochromatic domains enriched for methylated H3K9 (H3K9me) and lacking H3K4me[15] (Supplementary Figs. 3a). At telomeres, H3K9me is distributed across a ~100 kb domain (Fig. 1c), beyond the heterochromatin domain previously defined using a less sensitive method[15]. H2A.Z is depleted in this entire H3K9me-coated domain (Fig. 1c). *pht1* causes a slight increase in silencing at pericentromeric region but H3K9me distribution at heterochromatic loci is not severely altered (Supplementary Fig. 4a). At euchromatic loci, H2A.Z localizes preferentially in intergenic regions (Supplementary Fig. 3b) with maximum enrichment occurring ~200 bp upstream of translation start sites (Fig. 1d). This pattern is similar in other organisms[16–21], suggesting that this is a general feature of H2A.Z deposition. Comparison of H2A.Z and RNA polymerase II (Pol II) distributions revealed that *S. pombe* H2A.Z is preferentially enriched at repressed or weakly expressed genes (Supplementary Fig. 3c), as in *S. cerevisiae*[16–18].

To determine whether H2A.Z affects transcription, we monitored transcript levels from both strands using tiling arrays. Consistent with reports that most of the *S. pombe* euchromatin is transcribed[1,2], we detected widespread sense and antisense transcripts in wild-type cells. *pht1* caused only modest changes in sense transcription. The affected loci included subtelomeric genes such as *tlh2* sharing homology to centromeric repeats (Supplementary Fig. 4b). Silencing of *tlh2* and its paralogs requires heterochromatin machinery[7] (Supplementary Fig. 4b), butH2A.Z, undetected in our assays, may also contribute to *tlh2* repression.

pht1 caused a disproportionate increase in antisense transcripts at many (~5–8%) euchromatic loci (Fig. 1e–g; Supplementary Figs. 5), as confirmed by strand-specific RT-PCR (Fig. 1f). More than 90% of antisense RNAs mapped to convergent genes transcribed

from opposite DNA strands. These antisense RNAs appear to result from read-through transcription (Fig. 1g; Supplementary Figs. 6; see below). Since heterochromatin factors have been implicated in control of antisense transcripts[22], including read-through transcripts at three convergent loci[23], we asked whether H2A.Z interacts genetically with heterochromatin machinery. When *pht1* was combined with mutant alleles of *clr4* or *rik1*, components of Clr4-containing ClrC complex[7], the resultant double mutants displayed severe growth defects and a large, synergistic increase in antisense RNAs at >20% of genes (Fig. 2a; Supplementary Figs. 5, 7a–b). Consistent with ClrC directly participating in antisense suppression, Rik1 was found at the convergent loci (Supplementary Fig. 7c).

ClrC collaborates with RNAi factors including an Argonaute (Ago1)-containing RITS complex[24], to silence heterochromatic repeats[7]. We asked whether Ago1 contributes to antisense suppression. Combining *ago1* with *pht1* resulted in synergistic upregulation of antisense transcripts, as in *clr4 pht1* (Fig. 2a). These data are consistent with RNAi-dependent heterochromatin assembly, especially Swi6/HP1 bound to H3K9me, recruiting cohesin to mediate transcription termination[23]. However, antisense RNAs did not accumulate extensively in *swi6* cells and the synergistic increase in antisense RNAs observed in *clr4 pht1* mutant was not observed in the *swi6 pht1* mutant (Fig. 2a). Thus, ClrC and Ago1 contribute to antisense suppression via novel mechanism(s).

To gain insight into the roles of H2A.Z and heterochromatin/RNAi in antisense suppression, we examined common features of antisense RNAs in different mutants. Similar to *pht1*, most loci affected in *clr4 pht1* and *ago1 pht1* double mutants were convergent genes, including loci affected in the single mutants. The average profile of relative changes between mutant versus wild-type clearly demonstrates synergistic interactions of H2A.Z with Clr4 and Ago1 in suppressing antisense transcripts (Fig. 2c). The increase in antisense transcripts was not restricted to a specific region, but occurred uniformly throughout the gene body (Fig. 2c), consistent with read-through transcripts traversing adjacent loci (Supplementary Fig. 6). This is also illustrated in the average profile of antisense signal intensities (Fig. 2d). Examination of individual loci recapitulated the accumulation of ORF-spanning read-through antisense transcripts in double mutants (Fig. 2b).

Northern analyses confirmed that antisense RNAs observed in *pht1*, *clr4* and *clr4 pht1* mutants correspond to read-through transcripts rather than new initiation events. Strand-specific probes for antisense transcripts at *cyp7* or *srb4* hybridized to long RNAs that accumulated in mutant backgrounds (Fig. 3a; Supplementary Fig. 8). The length and direction of antisense RNA, as determined by oligo-targeted RNase H cleavage, was consistent with read-through transcripts originating at the promoter of the adjacent convergent gene. Long read-through transcripts were also detected with probes used to detect sense transcripts at the *c16H5.04-cyp7* and *c29A3.19-c18e5.02c* gene pairs (Fig. 3a and Supplementary Fig. 9a). Importantly, *pht1* and *pht1 clr4* mutants showed elevated levels of antisense transcripts, but sense transcripts were not upregulated (Fig. 3a). Thus, H2A.Z and ClrC appear to specifically suppress read-through antisense transcripts.

The accumulation of antisense RNAs could result from defects in transcriptional termination and/or processing. Although termination failure cannot be completely excluded, levels of

nascent antisense transcripts, as determined by transcription run-on assay, were not considerably affected in *pht1* or *pht1 clr4* mutant (Supplementary Fig. 9b). We hypothesized that H2A.Z and heterochromatin factors might selectively promote degradation of antisense RNAs. Indeed, aberrant transcripts including antisense RNAs are known to be degraded by the 3' to 5' exonuclease activity of nuclear exosome8,9,22, which also processes heterochromatic repeat transcripts targeted by ClrC22,25. Deletion of exosome subunit *rrp6* led to an antisense profile closely resembling that of *clr4 pht1*, with read-through antisense RNA covering entire ORFs at convergent genes (Fig. 3b). Striking similarities in levels and patterns of antisense RNAs in *clr4 pht1* and *rrp6* mutants were observed at individual loci (Fig. 3c). Similar analyses revealed a remarkable correlation of antisense RNA upregulation between *rik1pht1* or *ago1pht1* mutants and *rrp6* mutant (Fig. 4a). We conclude that read-through transcripts are produced in wild type cells, but are processed by the exosome in a manner dependent upon H2A.Z, ClrC and Ago1.

The histone deacetylase (HDAC) Clr6 complex suppresses antisense transcripts initiating from cryptic promoters via a mechanism involving H3K36 methyltransferase Set222,26. To compare distributions of antisense transcripts, we comprehensively profiled and correlated distributions of antisense RNAs in different mutants (Fig. 4b). *set1 pht1* mutant shows severe synthetic growth defects similar to *clr4 pht1*27 but did not exhibit cumulative upregulation of antisense RNAs. Correlation coefficients from pairwise comparisons of antisense profiles were used to perform hierarchical clustering (Fig. 4b), in which mutants were sorted according to similarities in their antisense profiles. Double mutants lacking Pht1 and Ago1 or ClrC subunits clearly belong to a distinct cluster that associated closely with *rrp6*. This cluster was separated from a second cluster that included *set2* and Clr6 complex mutants (Fig. 4b). Therefore, the effect of H2A.Z/ClrC on antisense RNAs is distinct from that of the HDAC Clr6.

This study implicates H2A.Z and heterochromatin factors in suppression of potentially deleterious antisense RNAs. H2A.Z nucleosomes might directly obstruct Pol II progression, or facilitate loading of factors involved in structural organization of chromosome, which in turn promotes RNA degradation by stalling Pol II. Alternatively, H2A.Z might signal to Pol II-associated exosome28 that transcription has escaped its natural termination and therefore produced an aberrant transcript (Fig. 4c). H2A.Z and ClrC (Rik1 subunit resembles cleavage and polyadenylation factor CPSF-A7) may be components of a RNA quality control mechanism, which stimulates exosome activity via exosome cofactors8. Indeed, the loss of Cid14 subunit of TRAMP, implicated in exosome stimulation8 causes accumulation of antisense RNAs (Fig. 4b), and the *Drosophila* homolog of H2A.Z mediates targeting of mRNA processing factors29. In addition to ClrC, Ago1 also collaborates with H2A.Z to suppress antisense RNAs. Drawing from analyses at centromeric repeats7, Ago1 and ClrC might cooperate not only to process antisense RNAs but also to influence local chromatin to block antisense transcription23. Exosome might contribute to degradation of RNAs targeted by RNAi/ClrC in a manner similar to mRNAs targeted by RISC30. Future studies will explore the interplay between chromatin and RNA processing factors in suppressing antisense RNAs.

Considering that H2A.Z localizes at the 5'end of genes in most eukaryotes16–21 and that heterochromatin factors are found in euchromatic regions of different species7, the involvement of H2A.Z and heterochromatin machinery in antisense suppression might be conserved in other species. Defects in RNA processing could result in genome instability and might be partially responsible for chromosome segregation defects observed in H2A.Z and heterochromatin-defective mutants7,13, similar to those seen in other mutants showing upregulation of antisense RNAs22.

METHODS SUMMARY

ChIP and ChIP-chip were performed as described previously15, except that hybridizations were performed as per manufacturer (Agilent) recommendation. Antibodies used were: FLAG (M2; Sigma), H3K9me2 (Abcam), Pol II (8WG16; Covance), and Myc (Santa Cruz). For transcriptome analyses, total RNA was extracted with Master Pure Yeast RNA Purification kit (Epicenter) and 5 ug of RNA was reverse transcribed and labeled with Superscript Indirect cDNA labeling kit (Invitrogen). Data analysis was performed as described in Methods online. Transcription run-on was performed as described previously23. Standard methods were used to perform Northern analysis. RT-PCR experiments were performed with one-step RT-PCR kit (Qiagen).

METHODS

Protein purification

Extracts were prepared from cells expressing H2A.Z-FLAG, Swr1–3xFLAG or Msc1–3xFLAG. Specifically, exponentially growing cells were resuspended in 2xHC buffer (200 mM HEPES [pH 7.4], 250 mM KCl, 2 mM EDTA, and 20% glycerol) supplemented with protease inhibitors, frozen and disrupted. Extracts were spun at $100\,000 \times g$, pre-cleared with IgG and FLAG tagged proteins recovered by incubation with anti-FLAG M2 slurry (Sigma) for 4 hours, washed 12 times with 1xHC buffer and eluted with FLAG peptide.

Mass spectrometry

Purified proteins were separated by SDS-PAGE and stained using SimpleBlue® (Invitrogen). Excised gel pieces were subjected to in-gel digestion using trypsin. Peptides extracted from the gel pieces were desalted using a C18 ZipTip (Millipore, Bedford, MA), lyophilized and resuspended in 16 μL of 0.1% trifluoroacetic acid (TFA) prior to analysis by microcapillary reversed-phase liquid chromatography-tandem mass spectrometry (LC-MS^2). Each sample (6 μl) was loaded onto an Agilent 1100 nano-capillary HPLC system (Agilent Technologies, Palo Alto, CA) equipped with a 10 cm integrated nanoRPLC-electrospray ionization (ESI) emitter column (made in house), coupled online with a linear ion-trap (IT) mass spectrometer (LTQ XP, ThermoElectron, San Jose, CA). After sample injection, a 20 min. wash with 98% mobile phase A (0.1% formic acid) was applied and peptides were eluted using a linear gradient of 2% mobile phase B (0.1% formic acid in acetonitrile) to 42% mobile phase B within 40 min. at a constant flow rate of 200μl/min. The seven most intense molecular ions in the MS scan were sequentially selected for collision-induced dissociation (CID) using normalized collision energy of 35%. The mass spectra were

acquired over a mass-to-charge (*m/z*) range of 350–1800. The ESI source capillary voltage and temperature were maintained at 1.5 kV and 200 °C, respectively. The MS data were searched against the UniProt *S. pombe* database downloaded from the European Bioinformatics Institute website (http://www.ebi.ac.uk/integr8) using SEQUEST (ThermoElectron) operating on a 10 node Beowulf parallel virtual machine computer cluster (Dell, Inc., Round Rock, TX). Up to two missed tryptic cleavage sites and oxidation of methionyl residues were allowed during the database search. Thresholds for legitimate peptide identifications were set as follows: minimum delta correlation (DC_n) 0.1 and charge state dependent cross correlation scores (X_{corr}) 2.0 for $[M+H]^{1+}$ 2.5 for $[M+2H]^{2+}$ and 3.0 for $[M+3H]^{3+}$.

Histone analysis

Cells expressing H2A.Z-FLAG were resuspended in NIB buffer (0.25 M sucrose, 15 mM Pipes [pH 6.8], 60 mM KCl, 15 mM NaCl, 5 mM $MgCl_2$, 1 mM $CaCl_2$, 0.8% Triton X-100) supplemented with protease inhibitors, 2 mM $ZnSO_4$, 10 ng/ml trichostatin A, and homogenized with glass beads. Cell pellets were collected by centrifugation at $11,000 \times g$ and histones extracted with 0.4 M H_2SO_4 and precipitated with trichloroacetic acid. H2A.Z was detected by Western analysis with FLAG M2 antibody.

ChIP and ChIP-chip

Chromatin immunoprecipitation was preformed as described previously[15]. Briefly, exponentially growing cells (5×10^8) were fixed in 3% paraformaldehyde and chromatin was subsequently crosslinked by treatment of cells with 10 mM dimethyl adipimidate. Cells were washed with phosphate buffered saline, resuspended in lysis buffer (50 mM Hepes/KOH [pH 7.5], 140 mM NaCl, 1 mM EDTA, 1% Triton X-100, 0.1% DOC) and homogenized with glass beads. Chromatin was sheared by sonication to fragments of 500–1000 bp, precleared with protein A slurry and immunoprecipitated with 2–4 μg of antibody. Immunoprecipitated chromatin was recovered by incubation with protein A or protein G slurry, washed extensively and reverse crosslinked by incubation at 65°C. Immunoprecipitated and DNA isolated from whole cell extract (WCE) were analyzed by multiplex PCR or subjected to microarray-based ChIP-chip analysis.

For ChIP-chip, ChIP and WCE DNA samples were amplified using random-primed PCR and resulting samples were labeled with either Cy5 (ChIP) or Cy3 (WCE) dyes. Equal amounts of ChIP and WCE labeled DNA were hybridized to a custom Agilent 4×44K *S. pombe* oligonucleotide array containing 43,987 probes of 60mer oligos, which represent alternately the plus and minus strands, tiling a large part of chromosome II at 50bp resolution. This array design also contains randomly spotted oligonucleotides that have no homology to the *S. pombe* genome but serve as controls for determining background signals. Hybridizations were performed according to Agilent recommended protocol. Microarrays were scanned using Agilent scanner (type-G2505B) with extended dynamic range, and data were extracted with Agilent feature extraction software (CHIP-v1_95_May07 protocol). Processed signals were normalized using combined rank consistency filtering with LOWES intensity normalization. PValueLogRatio that measures the significance of signal log ratio over systematic noise level of an individual spot were calculated by feature extraction

program and were used for subsequent analysis. Enrichment values were calculated as a ratio of Cy5 processed signal/ Cy3 processed signal. To reduce random background noise inherent in microarray data, we subjected the data to a limited sliding-window average filter and smoothed the data with sliding weighted average of three neighboring probes.

Expression profiling

Total RNA was isolated using Master Pure Yeast RNA purification kit (Epicenter). Invitrogen RiboMinus Yeast kit was used to partly deplete ribosomal RNA from samples before the reverse transcription (RT) step. RT was performed using random hexamer and anchored oligodT primer mix. 3 ug of RNA was labeled with Superscript Indirect cDNA labeling kit (Invitrogen). Labeled cDNA samples from mutant (Cy5) and wild type (Cy3) were mixed and hybridized to a high-density microarray, as described above. Data were extracted with Agilent Feature Extraction Software (GE2-v5_95_Feb07 protocol) and processed using combined rank consistency filtering with LOWES intensity normalization. Expression ratios were calculated as Cy5processed signal/Cy3processed signal. Ratios with non-significant P values (PValueLogRatio 0.05) were set to 1. Background signal was estimated as a median processed signal of 152 oligonucleotides with no homology to *S. pombe* genome, randomly spotted on array. Due to the column purification step in cDNA labeling method, very short transcripts (< 100–150 nucleotides), such as those described around the promoter regions in the *rrp6* mutant strains in *S. cerevisiae* and other systems, might not be recovered. However, analysis of our data reveals a specific increase in short transcripts upstream of promoter regions in particular in   *rrp6* cells, which is compatible with the recently reported results.

Average gene profiles

To calculate average gene profiles, 842 ORFs (region Chr2:1000000-Chr2:3049820) were aligned at 5' end or double aligned at 5' and 3' ends (see text). For double alignment, genes shorter than 1,650 bp were aligned without stretching. Genes longer than 1,650 bp were subjected to the following method: 14 probes from each end were included in dataset without any change while extra probes in the middle of gene body were linearly compressed into 5 points. Extremely short genes (<200 bp) were excluded from analysis. Intergenic regions upstream and downstream of ORFs were aligned according to translational start and stop sites, respectively. Probes represented in neighbor ORF were excluded. Intergenic probes within 1,000 bp region of both adjacent ORFs were included twice (once for each adjoined ORF), but weighted according to their distance from the ORFs. Repetitive probes (>80% homology with two or more chromosomal localization) were excluded from the averaging process. Expression profiles of genes (expression signal or expression ratio) were calculated similarly to the ChIP profiles with the exception that probes with multiple characteristics were weighted fully in the average.

Cross-correlation matrix and cluster analysis

Median antisense ratios (*mutant*/*wt*) for 842 genes (region Chr2:1000000-Chr2:3049820 – excluded the heterochromatic regions and repetitive probes) were calculated for each expression dataset. Linear regression analysis was carried out between datasets, and

Pearson-correlation index was calculated. *r* values were converted into color codes and plotted as a matrix. We repeated the analysis using the non-parametric Spearman's rank correlation coefficient, and observed very similar results (data not shown). Cluster analysis ("*average*" method in *hclust()* R function) was carried out for Euclidean distance of the *r* values between mutant strains.

Transcriptional run-on assay (TRO)

TRO was conducted essentially as described previously23. Fifty ml of exponentially growing culture was cooled and harvested at OD_{595nm}~ 0.2, washed with ice-cold TMN buffer (10 mM Tris/HCl pH 7.5, 5 mM $MgCl_2$, 100 mM NaCl) and resuspended in ice-cold water and supplemented with 10% N-lauryl sarcosine sulfate to a final concentration of 0.6%. Cells were incubated on ice for 25 min, pelleted and resuspended in 60 μl of 2.5x transcription buffer (50 mM Tris/HCl pH 7.5, 80 mM $MgCl_2$, 500 mM KCl, 5 mM DTT). Run was initiated by addition of 0.5 mM rATP, rCTP, rGTP supplemented with 200 μCi of α-P^{32}UTP and incubated at 30°C for 2 min. Reaction was stopped by addition of 1ml of ice-cold TMN, and cells were pelleted. RNA was isolated as for Northern Blot analysis, precipitated and before hybridization treated with 0.15 M NaOH on ice for 5 min, neutralized, mixed with hybridization solution (10 mM Tris/HCl pH 7.5, 82.5 μg/ml of yeast tRNA, 10x Denhardt's solution, 0.3 M NaCl, 10mM EDTA, 1% SDS, 0.5% BSA), heat-denatured and hybridized to 10 μg of RNA probes slot-blotted to BrightStar^R-Plus membrane at 65°C for 48 hours. After hybridization, membranes were washed twice at 65°C in 2xSCC supplemented with 1% SDS for 30 min.

Northern analysis

Total RNA was extracted from exponentially growing cells and Northern blot analysis conducted using the NorthernMax™ kit (Ambion). Probes were synthesized by *in vitro* transcription with α-P^{32}-UTP using the T7 MAXIscript kit (Ambion).

Supplementary Material

Refer to Web version on PubMed Central for supplementary material.

Acknowledgements

References

1. Wilhelm BT, et al. Dynamic repertoire of a eukaryotic transcriptome surveyed at single-nucleotide resolution. Nature. 2008; 453:1239–1243. [PubMed: 18488015]

2. Dutrow N, et al. Dynamic transcriptome of *Schizosaccharomyces pombe* shown by RNA-DNA hybrid mapping. Nat. Genet. 2008; 40:977–986. [PubMed: 18641648]

3. Cawley S, et al. Unbiased mapping of transcription factor binding sites along human chromosomes 21 and 22 points to widespread regulation of noncoding RNAs. Cell. 2004; 116:499–509. [PubMed: 14980218]

4. Martens JA, Laprade L, Winston F. Intergenic transcription is required to repress the *Saccharomyces cerevisiae* SER3 gene. Nature. 2004; 429:571–574. [PubMed: 15175754]

5. Hirota K, et al. Stepwise chromatin remodelling by a cascade of transcription initiation of non-coding RNAs. Nature. 2008; 456:130–134. [PubMed: 18820678]

6. Camblong J, Iglesias N, Fickentscher C, Dieppois G, Stutz F. Antisense RNA stabilization induces transcriptional gene silencing via histone deacetylation in *S. cerevisiae*. Cell. 2007; 131:706–717. [PubMed: 18022365]

7. Grewal SI, Jia S. Heterochromatin revisited. Nat. Rev. Genet. 2007; 8:35–46. [PubMed: 17173056]

8. Houseley J, LaCava J, Tollervey D. RNA-quality control by the exosome. Nat. Rev. Mol. Cell. Biol. 2006; 7:529–539. [PubMed: 16829983]

9. Wyers F, et al. Cryptic pol II transcripts are degraded by a nuclear quality control pathway involving a new poly(A) polymerase. Cell. 2005; 121:725–737. [PubMed: 15935759]

10. Guillemette B, Gaudreau L. Reuniting the contrasting functions of H2A.Z. Biochem. Cell Biol. 2006; 84:528–535. [PubMed: 16936825]

11. Swaminathan J, Baxter EM, Corces VG. The role of histone H2Av variant replacement and histone H4 acetylation in the establishment of *Drosophila* heterochromatin. Genes Dev. 2005; 19:65–76. [PubMed: 15630020]

12. Rangasamy D, Greaves I, Tremethick DJ. RNA interference demonstrates a novel role for H2A.Z in chromosome segregation. Nat. Struct. Mol. Biol. 2004; 11:650–655. [PubMed: 15195148]

13. Carr AM, et al. Analysis of a histone H2A variant from fission yeast: evidence for a role in chromosome stability. Mol. Gen. Genet. 1994; 245:628–635. [PubMed: 7808414]

14. Shevchenko A, et al. Chromatin Central: towards the comparative proteome by accurate mapping of the yeast proteomic environment. Genome Biol. 2008; 9:R167. [PubMed: 19040720]

15. Cam H, et al. Comprehensive analysis of heterochromatin- and RNAi-mediated epigenetic control of the fission yeast genome. Nat. Genet. 2005; 37:809–819. [PubMed: 15976807]

16. Raisner RM, et al. Histone variant H2A.Z marks the 5' ends of both active and inactive genes in euchromatin. Cell. 2005; 123:233–248. [PubMed: 16239142]

17. Zhang H, Roberts DN, Cairns BR. Genome-wide dynamics of Htz1, a histone H2A variant that poises repressed/basal promoters for activation through histone loss. Cell. 2005; 123:219–231. [PubMed: 16239141]

18. Li B, et al. Preferential occupancy of histone variant H2AZ at inactive promoters influences local histone modifications and chromatin remodeling. Proc. Natl. Acad. Sci. USA. 2005; 102:18385–18390. [PubMed: 16344463]

19. Whittle CM, et al. The genomic distribution and function of histone variant HTZ-1 during *C. elegans* embryogenesis. PLoS Genet. 2008; 4:e1000187. [PubMed: 18787694]

20. Mavrich TN, et al. Nucleosome organization in the *Drosophila* genome. Nature. 2008; 453:358–362. [PubMed: 18408708]

21. Zilberman D, Coleman-Derr D, Ballinger T, Henikoff S. Histone H2A.Z and DNA methylation are mutually antagonistic chromatin marks. Nature. 2008; 456:125–129. [PubMed: 18815594]

22. Nicolas E, et al. Distinct roles of HDAC complexes in promoter silencing, antisense suppression and DNA damage protection. Nat. Struct. Mol. Biol. 2007; 14:372–380. [PubMed: 17450151]

23. Gullerova M, Proudfoot NJ. Cohesin complex promotes transcriptional termination between convergent genes in *S. pombe*. Cell. 2008; 132:983–995. [PubMed: 18358811]

24. Zhang K, Mosch K, Fischle W, Grewal SI. Roles of the Clr4 methyltransferase complex in nucleation, spreading and maintenance of heterochromatin. Nat. Struct. Mol. Biol. 2008; 15:381–388. [PubMed: 18345014]

25. Murakami H, et al. Ribonuclease activity of Dis3 is required for mitotic progression and provides a possible link between heterochromatin and kinetochore function. PLoS ONE. 2007; 2:e317. [PubMed: 17380189]

26. Li B, Carey M, Workman JL. The role of chromatin during transcription. Cell. 2007; 128:707–719. [PubMed: 17320508]

27. Roguev A, et al. Conservation and rewiring of functional modules revealed by an epistasis map in fission yeast. Science. 2008; 322:405–410. [PubMed: 18818364]

28. Andrulis ED, et al. The RNA processing exosome is linked to elongating RNA polymerase II in *Drosophila*. Nature. 2002; 420:837–841. [PubMed: 12490954]

29. Wagner EJ, et al. A genome-wide RNA interference screen reveals that variant histones are necessary for replication-dependent histone pre-mRNA processing. Mol. Cell. 2007; 28:692–699. [PubMed: 18042462]

30. Orban TI, Izaurralde E. Decay of mRNAs targeted by RISC requires XRN1, the Ski complex, and the exosome. RNA. 2005; 11:459–469. [PubMed: 15703439]
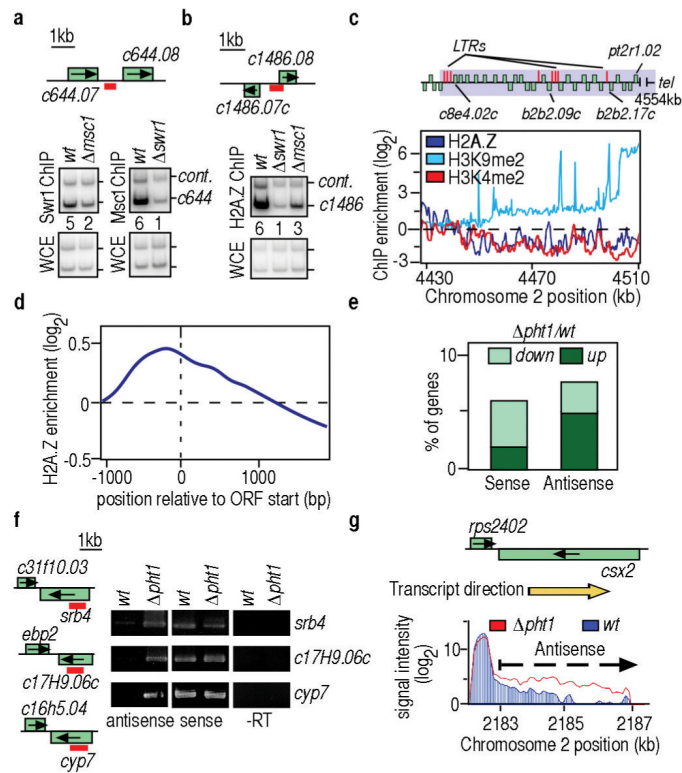
Figure 1. *pht1* **causes upregulated antisense transcripts**
a–b, H2A.Z is targeted preferentially to the 5' ends of genes. **a,** ChIP analysis of Swr1 and Msc1. DNA isolated from ChIP and whole cell extract (WCE) was analyzed by multiplex PCR. Control corresponds to gene-free region adjacent to *SPAC5H10.03*. Relative enrichment values are shown. **b,** H2A.Z deposition requires Swr1 and Msc1. **c,** H2A.Z is slightly enriched at heterochromatin domains. H3K4me15, H3K9me and H2A.Z distributions at a subtelomeric region. Note the LTR cluster demarcating the border of the H2A.Z depleted region. **d,** H2A.Z is enriched at 5' ends of genes. **e–g,** Upregulation of antisense transcripts at convergent genes in *pht1* cells. **e,** Percentage of genes with >2-fold altered median transcript levels in *pht1*. **f,** Strand-specific RT-PCR of RNAs isolated from *wt* and *pht1* cells. **g,** Transcripts at *rps2402/csx2* locus were examined by expression analysis using tiling microarray.
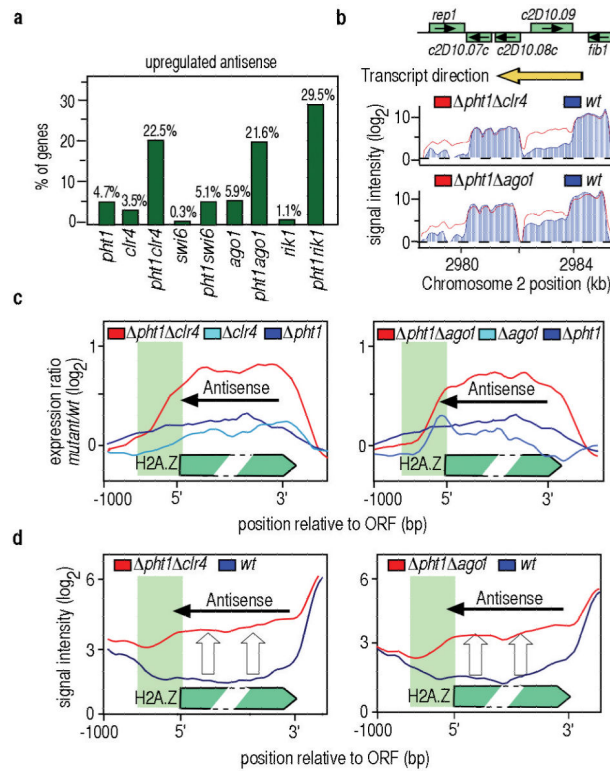
Figure 2. H2A.Z acts in synergistic manner with ClrC and Ago1 to suppress antisense transcripts

a, Cumulative derepression of antisense RNAs estimated as a percentage of genes with upregulated antisense. **b,** Representative examples with upregulated antisense in Δ*pht1* Δ*clr4* and Δ*pht1* Δ*ago1* mutants. Signal intensity of transcripts from reverse/lower strand is plotted. **c,** Profile of average antisense signal ratios at convergent genes in single (Δ*pht1/wt*, Δ*ago1/wt* and Δ*clr4/wt*) and double mutants (Δ*pht1* Δ*clr4/wt* and Δ*pht1* Δ*ago1/wt*). Double alignment at 5' and 3' ends of genes was applied and varied gene length compensated by compression of middle part of gene. H2A.Z localization is indicated in green. **d,** Cumulative profile of antisense transcripts in indicated strains. The average antisense signal profile was calculated for genes with increased levels of antisense in double mutants and compared with the profile in *wt*.
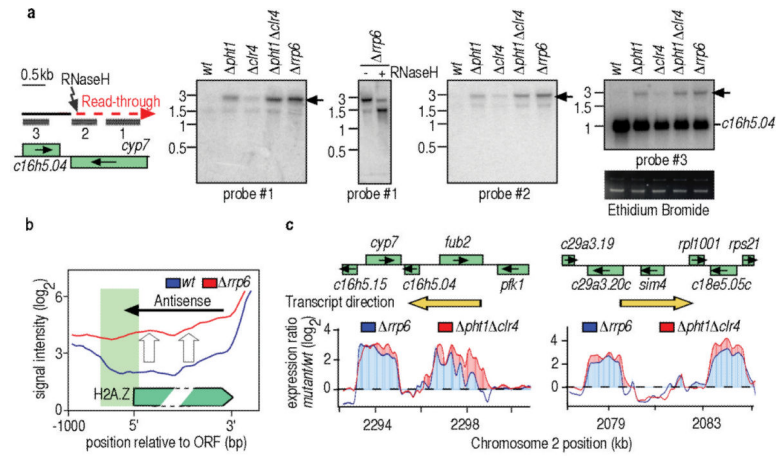
Figure 3. Read-through antisense transcripts are suppressed by the exosome

a, Antisense transcripts upregulated in *pht1 clr4* cells result from overlapping transcription at convergent genes. Northern analyses of RNAs at *SPBC16h5.04-cyp7*. Probes complementary to antisense (probe #1 and #2) and sense portion (probe #3) of *SPBC16h5.04* detected read-through transcripts. Oligonucleotide-targeted RNase H cleavage was used to determine 3' end of transcript. **b,** Cumulative profile of antisense transcripts in *rrp6* and *wt* cells. The antisense profile was calculated for genes with up-regulated antisense in *rrp6* cells and compared with *wt*. **c,** Expression profiling of antisense transcripts in *pht1 clr4* and *rrp6* cells.
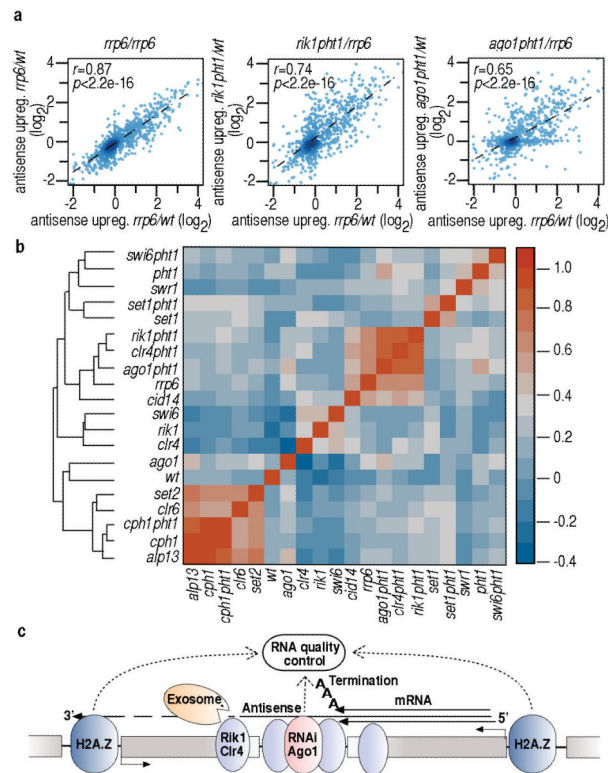
Figure 4. H2A.Z and heterochromatin factors suppress antisense RNAs targeted by the exosome
a, Density plot comparing upregulation of antisense transcripts in indicated mutants. Median antisense upregulation (*mutant*/*wt*) was calculated for 842 genes. Pearson's correlation coefficient (*r*) and the *p* value of the linear regression are indicated. Panel comparing antisense profiles of two *rrp6* mutants illustrates little variation between biological replicates. **b,** Hierarchical clustering of mutants based on similarities of their antisense profiles. Pairwise comparisons of antisense profiles were performed as in Fig. 4a and Pearson's correlation coefficients were converted into color codes. **c,** Model for antisense suppression at convergent genes. H2A.Z at the 5' ends of genes contribute to suppression of read-through transcripts that are degraded by exosome. Antisense suppression also requires ClrC and Ago1, which along with H2A.Z may facilitate loading of other factors to block Pol II progression23 and/or mediate the processing of RNAs by the exosome.